Proceedings of The ASME - JSME - KSME Joint Fluids Engineering conference 2019
AJKFLUIDS2019
July 28 - August 1, 2019, San Francisco, CA, USA

AJKFLUIDS2019-4617

EFFECT OF MICROSCOPIC VORTICES CAUSED BY FLOW INTERACTION WITH SOLID OBSTACLES ON HEAT TRANSFER IN TURBULENT POROUS MEDIA FLOWS

Ching-Wei Huang, Vishal Srikanth, Haodong Li, Andrey V. Kuznetsov*
Department of Mechanical and Aerospace Engineering
North Carolina State University
Raleigh, NC 27695-7910, USA

ABSTRACT

Turbulent flow in a homogeneous porous medium was investigated through the use of numerical methods by employing the Reynolds Averaged Navier-Stokes (RANS) modeling technique. The focus of our research was to study how microscopic vortices in porous media flow influence the heat transfer from the solid obstacles comprising the porous medium to the fluid. A Representative Elementary Volume (REV) with 4×4 cylindrical obstacles and periodic boundary conditions was used to represent the infinite porous medium structure.

Our hypothesis is that the rate of heat transfer between the obstacle surface and the fluid (q_{avg}) is strongly influenced by the size of the contact area between the vortices and the solid obstacles in the porous medium (A_{vc}). This is because vortices are regions with low velocity that form an insulating layer on the surface of the obstacles. Factors such as the porosity (φ), Pore Scale Reynolds number (Re_p), and obstacle shape of the porous medium were investigated. All three of these factors have different influences on the contact area A_{vc}, and, by extension, the overall heat transfer rate q_{avg}. Under the same Pore Scale Reynolds number (Re_p), our results suggest that a higher overall heat transfer rate is exhibited for smaller contact areas between the vortices and the obstacle surface. Although the size of the contact area, A_{vc}, is affected by Re_p, the direct influence of Re_p on the overall heat transfer rate q_{avg} is much stronger, and exceeds the effect of A_{vc} on q_{avg}. The Pore Scale Reynolds number, Re_p, and the mean Nusselt number, Nu_m, have a seemingly logarithmic relationship.

INTRODUCTION

Porous media are commonly used in heat exchangers to enhance thermal efficiency due to their high surface contact area per unit volume, which helps to enhance the heat transfer rate. Microscopic vortices, caused by flow interaction with solid obstacles, have a significant influence on heat transfer. We examine the characteristics of microscopic vortices and their influence on heat transfer in turbulent porous media flow.

Convection in porous media has been reviewed by Nield and Bejan [1], discussing factors such as pressure changes, viscous dissipation, and lack of local thermal equilibrium. Nakamura et al. [2] reported that for flow over a single cylinder, the relation between the Nusselt number and Reynolds number varies greatly for different flow regimes, which correspond to different lengths of the vortex formation region behind the cylinder. Similar correlations of the Nusselt number and Reynolds number were reported in studies of convection heat transfer for an array of obstacles. Direct numerical simulations were conducted for uniformly spaced squares, circular rods, and spheres by Kuwahara et al. [3]. McCarthy [4] performed Lattice gas cellular automata simulations for flow through arrays of cylinders. Although extensive work has been done for the macroscopic heat transfer in convection flow in porous media, the various effects of the microscopic vortices on heat transfer in different conditions have yet to be explored thoroughly.

METHODS

A Representative Elementary Volume (REV) was used in order to simulate an infinite periodic matrix. The REV is defined as the smallest sub-volume that shows the same behavior as the flow in the whole porous domain. Uth et al. [5] performed a DNS study of turbulent forced convection in porous media and reported that the largest scale of turbulence structures observed in their study was approximately four times the distance between centers of the obstacles, s. Thus, a REV with a side length of $4s$ is assumed to be a sufficiently large size to capture the largest turbulent eddies in the porous medium.

* Corresponding author, e-mail avkuznet@ncsu.edu

The REV is $4s \times 4s \times 2s$ in the x, y, and z-directions respectively, as shown in Fig. 1. The REV consists of 4×4 cylindrical obstacles whose center points are a distance s apart in the x and y-directions. In our computations, the porosity φ is varied from 0.800 to 0.497, while the Pore Scale Reynolds number Re_p varies from 50 to 5000. These parameters are defined as

$$\varphi = 1 - \frac{\pi}{4}\left(\frac{d}{s}\right)^2 \quad (1)$$

$$Re_p = \varphi \cdot \frac{u_{m,x} d}{\nu} \quad (2)$$

where d is the diameter of cylindrical obstacles, $u_{m,x}$ is the mean velocity in the x-direction, and ν is the kinematic viscosity of the fluid.

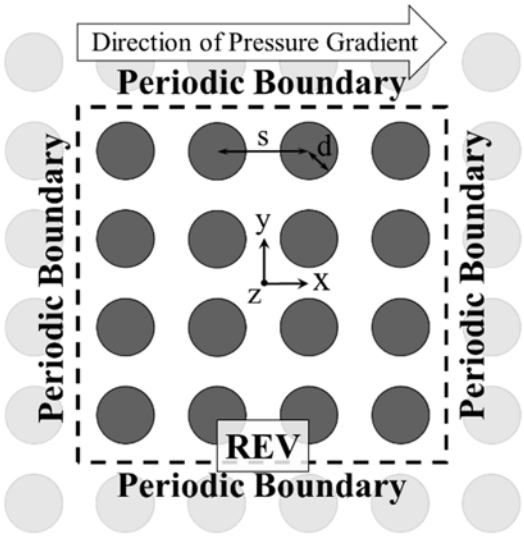

Fig. 1 The REV, marked by the dashed lines, for a homogeneous porous medium with infinite cylindrical obstacles. The distance between centers of the obstacles s and the obstacle diameter d are also shown in the figure.

Periodic boundary conditions were used in the x, y, and z-directions, respectively. A mass flow rate, $\dot{m}$, was specified in the x-direction to match the desired Pore Scale Reynolds number (Re_p). No-slip boundary conditions were used on the walls of cylindrical obstacles. The temperature of the walls of the cylindrical obstacles was set to a constant value of 353K, while the average temperature of the inlet flow was set to 323K. With this boundary condition setting, the characteristic temperature difference, ΔT, was 30K.

The turbulence model used in this study was the realizable k-ε model. Computations were performed using the commercial software ANSYS FLUENT 18.1 (ANSYS, Canonsburg, Pennsylvania) [6].

To validate our results, a Large Eddy Simulation (LES) study for a REV consisting of cylindrical obstacles was performed to verify results with the k-ε model at $\varphi = 0.497$ and $Re_p = 500$. The discussion comparing RANS and LES results is presented in the Reynolds Number section of Results and Discussion. A grid independence study was performed for the case of $\varphi = 0.497$ at $Re_p = 5000$ for cylindrical obstacles representing the porous medium. The y^+ values were kept at 1 near the walls while the maximum grid size was altered. RANS results were compared while decreasing the grid size until the changes of the applied pressure gradient and the average Nusselt number Nu_m were below 1%. Nu_m is defined as

$$Nu_m = \frac{\bar{h}d}{k} = \frac{q_{avg}}{k(\Delta T)/d} \quad (3)$$

RESULTS AND DISCUSSION

POROSITY

We investigated the influence of porosity on the microscopic vortices and, by extension, the effects of porosity on heat transfer between the obstacle surface and fluid (q_{avg}). The Pore Scale Reynolds number was kept constant at $Re_p = 5000$ and the porosity was varied by adjusting the distance between neighboring obstacles s.

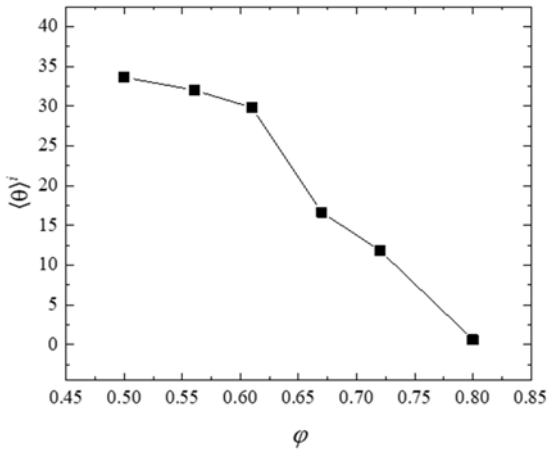

Fig. 2. Variation of macroscopic flow angle $\langle\theta\rangle^i$ with porosity for circular cylindrical obstacles.

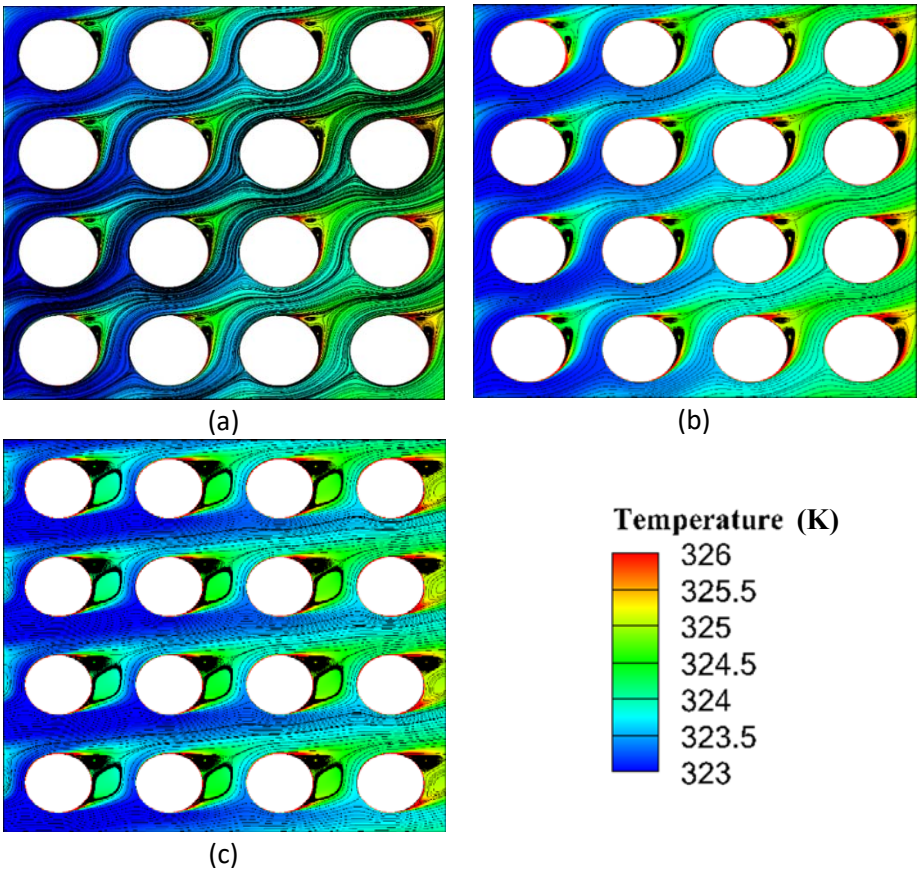

Fig. 3. Streamlines and temperature distribution obtained from RANS results in the midplane of the REV. $Re_p = 5000$, $\Delta T = 30\text{K}$ (a) $\varphi = 0.600$ (b) $\varphi = 0.650$ and (c) $\varphi = 0.717$.

As reported by Srikanth et al. [7], a symmetry breaking phenomenon is shown to occur in turbulent flow in porous media with low porosity. After the symmetry breaking occurs, the macroscopic flow deviates from the direction in which the pressure gradient is applied, forming a macroscopic flow angle $\langle\theta\rangle^i$, which is defined as the angle between the direction of the applied pressure gradient and the volume average flow direction. The variation of macroscopic flow angle $\langle\theta\rangle^i$ with porosity is shown in Fig. 2. This phenomenon results in different vortex patterns forming in the porous medium flow as $\langle\theta\rangle^i$ varies, as shown in Fig. 3. The magnitude of the deviation is strongly influenced by the porosity of the porous medium. As the porosity decreases from unity, the macroscopic flow angle $\langle\theta\rangle^i$ increases.

The macroscopic flow angle exhibits a sudden increase as the porosity decreases from 0.65 to 0.6, then slightly increases as the porosity decreases further. At higher porosities ($\varphi > 0.800$), the average flow direction generally stays in the same direction of applied pressure gradient ($\langle\theta\rangle^i = 2.3 \times 10^{-5}$). As the porosity decreases ($0.497 < \varphi < 0.717$), the direction of the average flow starts to deviate from the direction of applied pressure gradient. In this range of porosity, the shape of the wake behind each obstacle changes with respect to the change in the macroscopic flow angle. The vortices inside the wake are regions with a low velocity that form an insulating layer on the surface of the obstacles, affecting heat transfer from the area of contact between the vortices in the wake and the surface of an obstacle (A_{vc}). A_{vc} is defined as

$$A_{vc} = A_{wake}/A_{total} \tag{4}$$

where A_{wake} is the area of the wake in contact with the obstacle (between the two separation points on the obstacle) and A_{total} is the total surface area of the obstacle. The increase in the macroscopic flow angle leads to a decrease in A_{vc}.

Due to the nature of the flow interaction with the obstacle walls, larger vortices are formed during the transition between minimum to maximum deviation, which leads to a decrease in the heat transfer rate during the transition. Once the deviation of the flow from the direction in which the pressure gradient is applied reaches its highest value, the vortex separation point on one side of the obstacle is pushed downstream, resulting in the contact area between the vortices and the obstacle surface to decrease. Consequently, the heat transfer rate increases. The heat transfer rate at maximum deviation, having a smaller contact area A_{vc}, is higher than that for the case with zero deviation, showing that the observed phenomenon can help to increase the rate of heat transfer in porous media under certain conditions. The

corresponding macroscopic flow angle, $\langle\theta\rangle^i$, and contact area between the wake and obstacle, A_{vc}, for various values of porosity, φ, are shown in Table 1.

The correlation of the average heat flux on the surfaces of the obstacles in the REV (q_{avg}) and the contact area between the wake vortices and the obstacle surface (A_{vc}) is shown in Fig. 4. The heat flux, q_{avg}, increases as the contact area, A_{vc}, decreases. We anticipate that q_{avg} reaches an upper limit as A_{vc} decreases to zero. This result supports our hypothesis that the vortices are regions with low velocity that form an insulating layer on the surface of the obstacles.

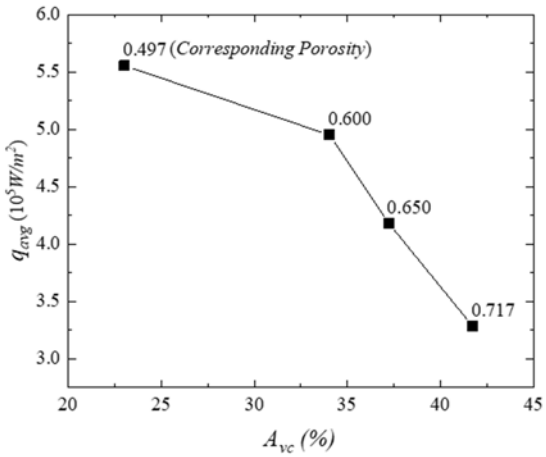

Fig. 4. Correlation between the average heat flux on surfaces of the obstacles in the REV (q_{avg}) and the contact area between the wake vortices and the obstacle surface (A_{vc}). The corresponding porosity is labeled for each data point.

φ	0.497	0.600	0.650	0.717
$\langle\theta\rangle^i$	33.63°	29.81°	16.63°	11.82°
A_{vc}	0.230	0.340	0.372	0.417

Table 1. Macroscopic flow angle, $\langle\theta\rangle^i$, and contact area between the wake and obstacle, A_{vc}, for various values of porosity, φ.

There are two main vortices forming in the wake of each obstacle, with the top vortex being slightly smaller than the bottom vortex. To measure the size of the top and bottom vortices in the wake, we define the non-dimensional Vortex Core diameter, d_v, as follows. Drawing a straight line between the top and bottom vortex cores (located using the maximum vorticity magnitude), there is a point of minimum vorticity, $P_{contact}$, on this line. $P_{contact}$ corresponds to a location where the top and bottom vortices are in contact. The vortex radius is defined as the distance between the vortex core and $P_{contact}$. The obstacle diameter is used to non-dimensionalize the Vortex Core diameter. The variation of d_v with porosity is shown in Fig. 5.

The size of the vortices, measured by d_v, stays relatively constant for $\varphi < 0.600$ and increases with the increase of porosity between $0.600 < \varphi < 0.717$. The ratio of the diameters of the top and bottom vortices is independent of the value of porosity for $0.600 < \varphi < 0.717$. For $\varphi > 0.800$, the average flow direction does not deviate from the driving force direction and the sizes of the top and bottom vortices become equal. More investigation is needed to verify the relation between the porosity and vortices inside the wake.

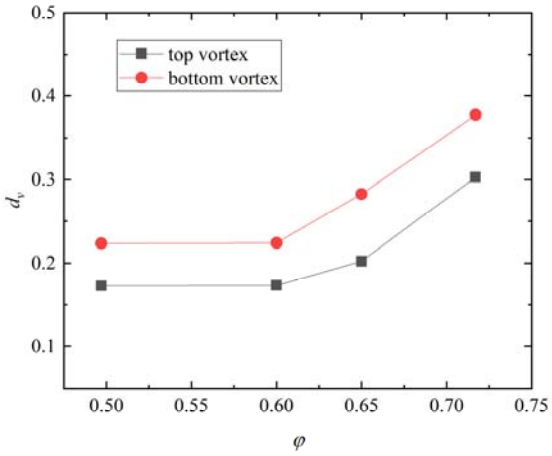

Fig 5. Variation of the Vortex Core Diameter, d_v, of the top and bottom vortices in the wake versus porosity, φ.

OBSTACLE SHAPE

Different shapes of obstacles composing a porous medium result in different flow patterns in a porous media flow, with flow separation happening on sharper edges of the obstacle wall. Under the conditions of $\varphi = 0.497$, $Re_p = 5000$, and $\Delta T = 30$K, the results for two homogeneous porous media consisting of either circular or square cylinders are vastly different. The streamlines and temperature distributions for these two cases are shown in Fig. 6.

The case of a porous medium composed of circular cylinders has two vortices in the wake of each cylinder that are attached to the obstacle surface, with a contact area $A_{vc} = 23\%$ and the average heat flux $q_{avg} = 5.554 \times 10^5 \ W/m^2$, as shown in Fig. 6(a). In the case of a porous medium comprised of square cylinders, a square obstacle is in contact with four vortices, located in the gaps between the upstream and downstream obstacles, as shown in Fig. 6(b). The vortices for the square obstacle case form a flow similar to that of a lid driven cavity, with a total contact area on an obstacle of $A_{vc} = 50\%$, and the average heat flux of $q_{avg} = 4.723 \times 10^5 \ W/m^2$. In the case of cylindrical obstacles, the primary flow in the porous medium weaves around the obstacles. As our hypothesis suggests, the size of the contact area between the vortices and the obstacle surface, A_{vc}, correlates with the heat transfer between the obstacles and porous media flow.

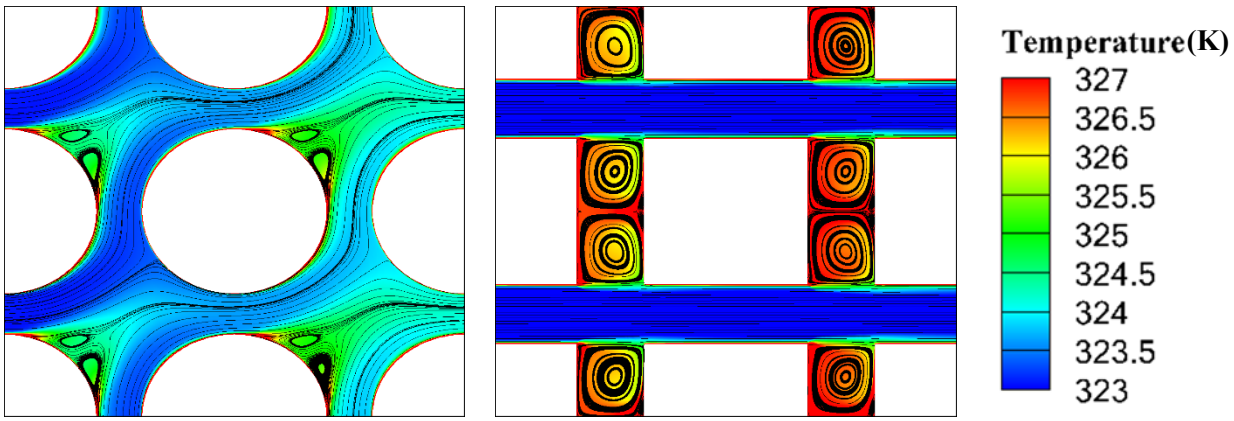

(a) (b)

Fig. 6. Streamlines and the temperature distribution obtained from RANS results in the midplane. Porous media flow in (a) A porous medium comprised of circular cylinders, (b) A porous medium comprised of square cylinders. $\varphi = 0.497$ and $Re_p = 5000$.

REYNOLDS NUMBER

At low Reynolds numbers ($Re_p < \sim 100$) in the laminar flow regime, the phenomenon of flow deviation from the direction of the applied pressure gradient does not occur, and the flow remains parallel to the direction of the pressure gradient. This forms large vortices between neighboring obstacles in the *x*-direction. As the flow transitions from laminar to turbulent somewhere between $50 < Re_p < 500$, the flow pattern changes with the change of the Reynolds number, resulting in smaller vortices attached to the obstacles as the macroscopic flow angle, $\langle\theta\rangle^i$, deviates from zero. Our numerical finding that the flow transition happens between $50 < Re_p < 500$ is supported by de Lemos [8] and Kaviany [9], who stated that flow in porous media is fully turbulent at $Re_p = 300$.

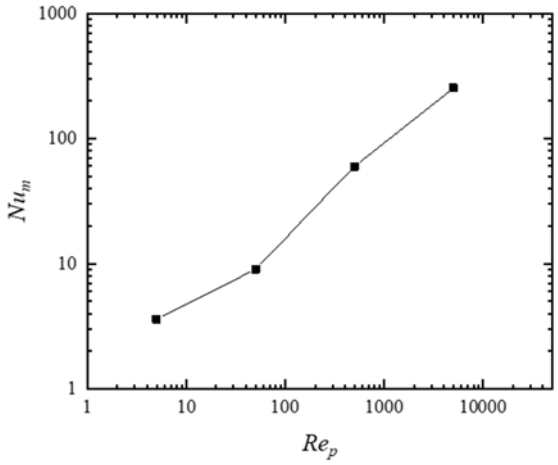

Fig. 7. Correlation between the Pore Scale Reynolds number Re_p and mean Nusselt number Nu_m on the top left obstacle in the REV.

Although our hypothesis states that the areas of the obstacle surface in contact with wake vortices will have a lower heat transfer rate compared to the areas in contact with the primary flow, the effect of this is small compared to the effect of the Reynolds number, Re_p, on the overall heat flux, q_{avg}. The correlation between the Pore Scale Reynolds number, Re_p, and the mean Nusselt number, Nu_m, of an obstacle is shown in Fig. 7. The slight change of the correlation between Re_p and Nu_m between $(50 < Re_p < 500)$ is likely due to the wake developing into a complex three-dimensional flow in this flow regime.

	RANS	LES(time averaged)
$\langle\theta\rangle^i$	32.903°	32.875°
$u_{m,x}$	0.1258	0.1296
$u_{m,y}$	0.0814	0.0837
Nu_m	59.953	72.650

Table 2. Comparison of RANS and time averaged LES results at $\varphi = 0.497$ and $Re_p = 500$. Here $u_{m,x}$ and $u_{m,y}$ are the mean velocities in the *x*-and *y*-directions, respectively, and $\langle\theta\rangle^i$ is the macroscopic flow angle, defined as $\tan^{-1}(u_{m,y}/u_{m,x})$.

An LES simulation was performed for $\varphi = 0.497$ and $Re_p = 500$. The time averaged LES solution in the REV mid-plane is shown in Fig. 8 and a comparison between the RANS and LES solutions is shown in Table 2. The discrepancy between the Nu_m of the RANS and LES cases are caused by the vortex shedding off the obstacle walls in the LES case, which is absent in the steady RANS simulation. Energy "packages" are delivered from the obstacle wall to the primary flow as the vortices are shed off the wall. This mechanism enhances heat exchange between the obstacle wall and the primary flow, and is

responsible for the higher Nu_m for the LES case compared to the RANS case (Table 2).

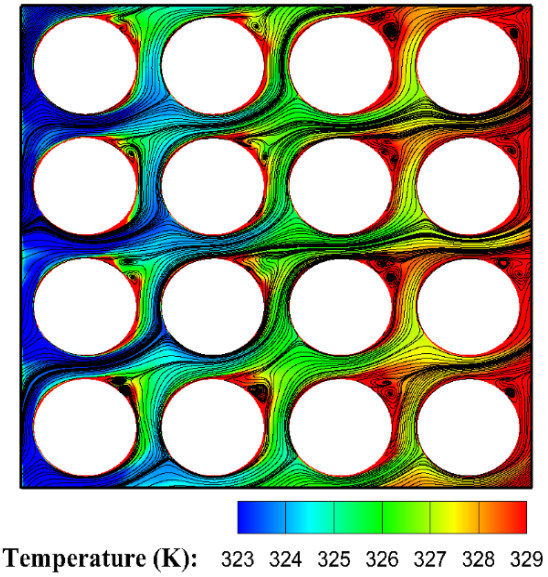

Fig. 8 Streamlines and the temperature distribution obtained from the time averaged LES results in the midplane of the REV. $Re_p = 500$, $\Delta T = 30$K, and $\varphi = 0.497$.

CONCLUSIONS

The results of our simulations support the hypothesis that the rate of heat transfer between the obstacle surface and the fluid is influenced by the size of the contact area of the vortices that are attached to the solid obstacles in the porous medium. The phenomenon of flow deviation from the driving force direction is shown to help increase the rate of heat transfer in porous media under certain conditions.

Although the contact area between the vortices and the obstacle surface, A_{vc}, has a considerable effect on the overall heat transfer from the obstacle to the fluid, it is not as significant compared to the effect of the Pore Scale Reynolds number Re_p. However in practice, increasing the Reynolds number requires using a larger applied pressure gradient to drive the flow faster. Our results show that by manipulating the vortex contact area with the obstacle by modifying such parameters as the obstacle shape or porosity while keeping the Reynolds number the same, the overall heat transfer rate between the obstacles and fluid can be increased in an "economical" way, without increasing the applied pressure gradient.

More DNS and LES studies are needed to gain a further understanding into the effect of turbulent vortices on heat transfer in porous media.

ACKNOWLEDGMENTS

AVK acknowledges with gratitude the support of the National Science Foundation (award CBET-1642262), the Alexander von Humboldt Foundation through the Humboldt Research Award, and the Extreme Science and Engineering Discovery Environment (XSEDE), which is supported by National Science Foundation grant number ACI-1548562.

REFERENCES

[1] Nield, D. A.; Bejan, A. (2017). *Convection in Porous Media* (5th ed.), Springer, New York. doi:10.1007/978-3-319-49562-0

[2] Nakamura, H.; Igarashi, T. (2004). Variation of Nusselt number with flow regimes behind a circular cylinder for Reynolds numbers from 70 to 30000, *International Journal of Heat and Mass Transfer*, Vol. 47, No. 23, 5169–5173. doi:10.1016/j.ijheatmasstransfer.2004.05.034

[3] Kuwahara, F.; Nakayama, A. (1998). Numerical Modeling of Non-Darcy Convective Flow in a Porous Medium, *Heat Transfer Proc.11th IHTC*, Vol. 4, 411–416

[4] McCarthy, J. F. (1994). Flow through arrays of cylinders: Lattice gas cellular automata simulations, *Physics of Fluids*, Vol. 6, No. 2, 435–437. doi:10.1063/1.868341

[5] Uth, M.-F.; Jin, Y.; Kuznetsov, A. V.; Herwig, H. (2016). A direct numerical simulation study on the possibility of macroscopic turbulence in porous media: Effects of different solid matrix geometries, solid boundaries, and two porosity scales, *Physics of Fluids*, Vol. 28, No. 6, 065101. doi:10.1063/1.4949549

[6] ANSYS Inc. (2018). *Fluent User's Guide* (Release 1.)

[7] Srikanth, V.; Huang, C. W.; Su, T. S.; Kuznetsov, A. V. (2018). Symmetry Breaking in Porous Media as a Consequence of the von Karman Instability. url:https://arxiv.org/abs/1810.10141

[8] de Lemos, M. J. S. (2012). *Turbulence in Porous Media: Modeling and Applications*, *Elsevier Inc.*, Elsevier, Instituto Tecnológico de Aeronáutica—ITA, Brazil. doi:10.1016/C2011-0-06981-8

[9] Kaviany, M. (1991). *Principles of Heat Transfer in Porous Media*, Springer US, New York, NY. doi:10.1007/978-1-4684-0412-8